A Compact Numerical Model for Photodetectors Made from Two-Dimensional Materials

Ergun Simsek and Raonaqul Islam

Department of Computer Science and Electrical Engineering (CSEE),
University of Maryland, Baltimore County, Baltimore, Maryland, USA.

ABSTRACT

This work presents a numerical investigation into the performance metrics of photodetectors made from monolayer MoS_2, a two-dimensional material with unique optoelectronic properties. The study introduces a one-dimensional drift-diffusion framework and wave propagation in layered media analysis. Results demonstrate a peak quantum efficiency at 561 nm, influenced by the substrate. The precision of the model validates its utility for characterizing MoS_2 photodetectors, emphasizing the importance of background inclusion in calculations. The efficiency of the computation makes the model suitable for in-depth device analyses and device design via numerical optimization.

Keywords: 2D materials, photodetectors, monolayer MoS_2, quantum efficiency, drift-diffusion model.

1. INTRODUCTION

A specific class of materials called transition metal dichalcogenides (TMDs), which contains one atom of transition metal and two chalcogen atoms, can be obtained as mono or a few layers.[1–6] Monolayer TMDs have attracted researchers' attention during the last two decades for various optoelectronic applications[3–5] due to their unique optical and electronic properties.[7–10] So far, the most commonly studied monolayer TMD has been the molybdenum disulfide (MoS_2).[1,2,8–14] When bulk MoS_2 is transformed into its monolayer counterpart, it becomes a direct-bandgap material, which means its valence band maximum and conduction band minimum have the same crystal momentum. Because of the direct bandgap, a photon can directly generate an electron-hole pair and hence monolayer MoS_2 can be used in photodetection applications.[6,14–16]

The ability of MoS_2-based phototransistors to convert optical excitations into electrical currents depends on numerous factors, including the quality, dimensions, doping, and defect levels of the two-dimensional (2D) material;[13] the materials and thicknesses of the substrate;[11] the type, shape, and placement of the metal contacts;[17] ambient temperature; wavelength and strength of the optical excitation;[2,4] and applied voltages.[5] Given the multitude of these variables, numerical methods can offer more precise designs for application-specific phototransistors compared to approximate analytical formulas. Ueda *et al.*, for instance, analyzed the carrier distributions in a monolayer tungsten diselenide (WSe_2) transistor covered with an ionic liquid by solving the drift-diffusion equations in two dimensions, marking the first known study on ion-gated transistor devices made from 2D materials.[15] Similarly, Chen *et al.* developed a numerical method combining the drift-diffusion transport equations with a 2D Poisson equation to simulate a 2D device structure.[16] Both studies produced results consistent with experimental data in the literature.

In this work, we propose a simplified one-dimensional (1D) numerical solution that is capable of solving the drift-diffusion model to determine the performance metrics of 2D material-based photodetectors. Here, we have chosen monolayer MoS_2 as the photosensitive layer to characterize the device but the theory is valid for other phototransistors made from thin TMD films. We have sequentially calculated the output current, quantum efficiency, phase noise, and bandwidth of the device. We validate our numerical results with the experimental results found in the literature.

Further author information: (Send correspondence to E. Simsek)
E. Simsek: E-mail: simsek@umbc.edu, Telephone: 1 (410) 455-3540
R. Islam: E-mail: raonaqi1@umbc.edu, Telephone: 1 (667) 910-4461

2. DEVICE STRUCTURE

Figure 1 shows the structure of the characterized device. It consists of a 0.65 nm thin MoS_2 monolayer on top of a 270 nm SiO_2 coated p-doped silicon substrate. There are two gold (Au) contacts at both sides of the monolayer, which connect the 2D material to the external circuit, as shown in Fig. 1(b). A bias voltage (V_d) is applied between the drain and source contacts. Another voltage is applied from the bottom of the device called the gate voltage (V_g). It is considered that the device is normally illuminated from the top. The device considered in this work is 1 μm long and 1 μm wide for all our simulations except the evaluation of radio frequency (RF) output power.

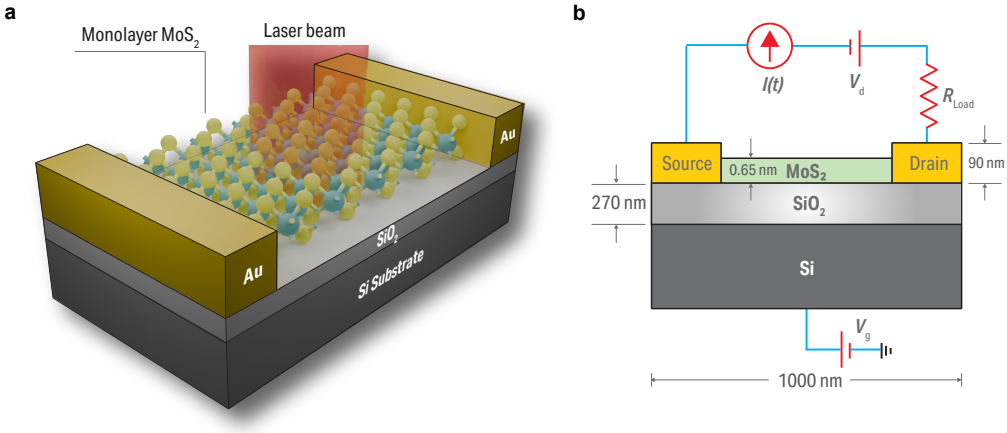

Figure 1. Schematic diagram of the monolayer MoS_2 based photodetector.

3. NUMERICAL MODEL

To determine the current transport behavior of the device, we use the drift-diffusion model.[6,18,19] We solve the current continuity equations self-consistently with Poisson's equation which are given as follows:

$$\frac{\delta(n-N_{\rm D}^{+})}{\delta t} = G - R(n,p) - \frac{\nabla\cdot\mathbf{J}_{\rm n}}{q}, \qquad \frac{\delta(p-N_{\rm A}^{-})}{\delta t} = G - R(n,p) + \frac{\nabla\cdot\mathbf{J}_{\rm p}}{q}, \qquad \nabla\cdot\mathbf{E} = \frac{q}{\varepsilon}(n-p+N_{\rm A}^{-}-N_{\rm D}^{+}), \quad (1)$$

where, q is the charge of electron, G is optical generation rate of the MoS_2 layer, R is the recombination rate, ε is the permittivity of MoS_2, and $N_{\rm D}^{+}$ and $N_{\rm A}^{-}$ are the ionized donor and acceptor impurity concentrations. $\mathbf{J}_{\rm n}$ and $\mathbf{J}_{\rm p}$ are current densities for electrons and holes, which are determined with the drift-diffusion equations, $\mathbf{J}_{\rm n} = qn\mathbf{v}_{\rm n}(\mathbf{E}) + qD_{\rm n}\nabla n$ and $\mathbf{J}_{\rm p} = qp\mathbf{v}_{\rm p}(\mathbf{E}) - qD_{\rm p}\nabla p$, where, $D_{\rm n} = k_BT\mu_n/q$ and $D_{\rm p} = k_BT\mu_p/q$ are the electron and hole's diffusion coefficients respectively. $\mathbf{v}_{\rm n}(\mathbf{E})$ and $\mathbf{v}_{\rm p}(\mathbf{E})$ are electric-field dependent electron and hole drift velocities respectively. The generation rate (G) of the MoS_2 layer is determined from the relation $G = P_0\alpha/AE_{\rm ph}$, where P_0 is the factor corresponding to incident laser power, α is the absorption coefficient of MoS_2 that is derived from the complex electrical permittivity, A is the illuminated surface area of the 2D material layer, and $E_{\rm ph}$ is the energy of incident photons.

To incorporate the applied gate voltage, we have considered the MoS_2 monolayer as intrinsically n-doped due to surface traps with a doping density of $N_{\rm traps}$, where $N_{\rm traps}$ is set equal to 10^{10} cm^{-2}. If V_g is more significant than a threshold value, *i.e.*, if $V_{\rm g} > V_{\rm th}$, then we calculate the doping density with the following expression: $n_{\rm s} = \varepsilon_{\rm ox}(V_{\rm g} - V_{\rm th})/t_{\rm ox}$, where $V_{\rm th} = N_{\rm traps}t_{\rm ox}/\varepsilon_{\rm ox}$, $t_{\rm ox}$ is the thickness of the oxide layer, and $\varepsilon_{\rm ox}$ is the permittivity of the oxide layer. The resistance, $R_{\rm Load}$ is calculated using $R_{\rm Load} = \sqrt{\rho_i \times R_{\rm sh}}$, where $R_{\rm sh}$ is the sheet resistance of the MoS_2 monolayer, $R_{\rm sh} = 1/qn\mu_n(T)A$, and ρ_i is the interfacial resistance between the contact and the MoS_2, with T being the temperature and μ_n is the electron low-field mobility. We calculate the interfacial resistance using an empirical formula ($\rho_i = 1/[(T-100)/107]^3$) derived from the experimental data.[20] Since we require the material properties of monolayer MoS_2 to solve for the current continuity and Poisson's

equations, we have gathered these material parameters from the literature. Table 1 lists material parameters used in this work. Moreover, we have utilized a hybrid Drude-Lorentz-Gaussian model to accurately determine the permittivity of monolayer MoS_2 as described in detail in Ref. 8.

Table 1. Material parameters of MoS_2 at $T = 300K$ used in our simulations. m_0 is the electron mass.

Parameter Name	**Symbol**	**Value**
Energy bandgap[9]	E_{g}	1.87 eV
Electron's effective mass[10]	m_{e}^*	$0.35m_0$
Hole's effective mass[10]	m_{h}^*	$0.50m_0$
Electron affinity[21]	χ_i	4.27 eV
Radiative recombination coefficient[12]	B_{r}	10^{-7} cm^3/s
Auger coefficient[12]	$C_{\mathrm{n}}, C_{\mathrm{p}}$	10^{-24} cm^6/s
Density of states in conduction band[22]	N_{C}	3.76×10^{11} cm^{-2}
Density of states in valence band[22]	N_{V}	5.76×10^{11} cm^{-2}
Hole saturation velocity[13]	$v_{\mathrm{p,sat}}$	1×10^7 cm/s
Electron saturation velocity[13]	$v_{\mathrm{n,sat}}$	4.2×10^6 cm/s
Electron lifetime[16]	τ_{n}	1×10^{-9} s
Hole lifetime[16]	τ_{p}	1×10^{-8} s

This model has three unknown parameters: electron density n, hole density p, and the electrical potential, ϕ. We use Newton's method to determine these three unknowns from three sets of equations. We solve for this model in two steps. Initially, we find the steady-state output current by using some initial guess for p, n, and ϕ. Then, we use the steady-state solution as an initial guess to find the dynamic output current in the time domain. The MoS_2 monolayer is first divided into uniform mesh points, and the second-order finite differences are used to discretize the parameters. We have used the implicit Euler method to obtain the solution in the time domain. Additionally, we consider our device a multilayered structure and assume that the incident wave is a plane wave. By solving for simple plane wave propagation in a layered medium, we find the local electric field inside the monolayer MoS_2. This electric field is used in our drift-diffusion solver to calculate the quantum efficiency of the device accurately. The solver is implemented in MATLAB. Each of the simulations takes less than two minutes on a desktop computer.

4. RESULTS AND DISCUSSION

We investigate the output current characteristics of the device as follows. First, we gradually increase the bias voltage (V_d), keeping the gate voltage (V_g) constant at 10 V. The illumination wavelength is set at 561 nm. It is shown in Fig. 2 (a) that output current increases and becomes saturated. When the illumination intensity is high, the output current gets saturated for a larger V_d. This is because, under low-intensity illumination, the carriers generated due to doping cause the current flow, and the current is saturated when these carriers reach their saturation velocities. However, in addition to doping at higher intensity, we have photogenerated carriers that enhance the output current and shift the saturation. In Fig. 2 (b), we keep V_d constant at 0.5 V and gradually increase V_g. When V_g is increased, the carrier density in MoS_2 monolayer is also increased, resulting in higher output current, which also saturates at some threshold value. Nevertheless, higher illumination intensity enables photogenerated electron-hole pairs to increase the output current further, as observed from different colored lines in Fig. 2 (b).

We next analyze the quantum efficiency (Q_{eff}) of the device. Q_{eff} is defined as the ratio between the number of electrons to the number of incident photons. Since we have obtained the output current in the time domain, its numerical integration over excitation time gives us the number of photogenerated electrons. We calculate the number of photons using the illumination intensity and the generation rate of monolayer MoS_2. Calculated Q_{eff} as a function of illumination wavelength is shown in the left y-axis of Fig. 3(a). It is observed that the Q_{eff} gradually increases with wavelength, reaches its peak around 561 nm, then decreases with further increase in wavelength. The experimental results[7] are denoted by the red dots aligned with the right y-axis. It is important

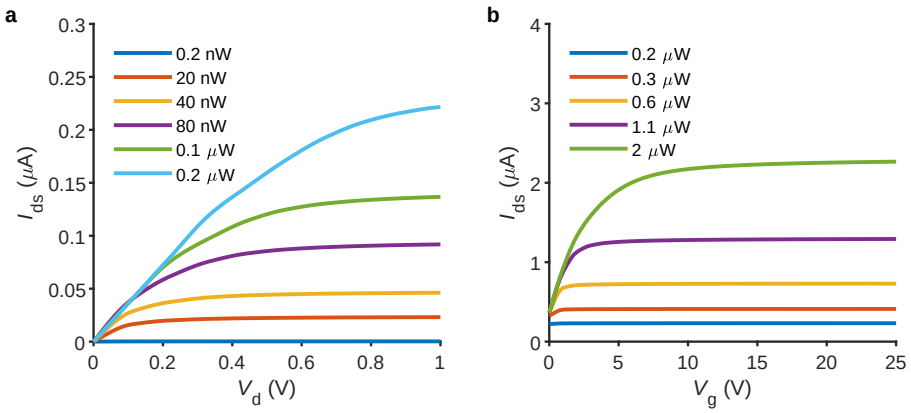

Figure 2. Output current as a function of a) bias voltage when $V_g = 0.5$ V and b) gate voltage when $V_d = 10$ V at different illumination intensities and $\lambda = 561$ nm.

to note that the scales of the experiment are different from our calculations because they measured internal quantum efficiency, which only considers the photons absorbed by the monolayer MoS_2. Nevertheless, we can observe from Fig. 3 (a) that our numerically calculated Q_{eff} shows a similar trend as the experiments. This trend is mainly controlled by the intensity of the electric field experienced by the MoS_2. Hence, taking substrate into account by following a wave propagation in layered media formalism is essential.[6,11] We have also analyzed Q_{eff} as a function of the input power. It is observed from Fig. 3 (b) that Q_{eff} is reduced with increased normalized power because the output current does not increase with incident power linearly.

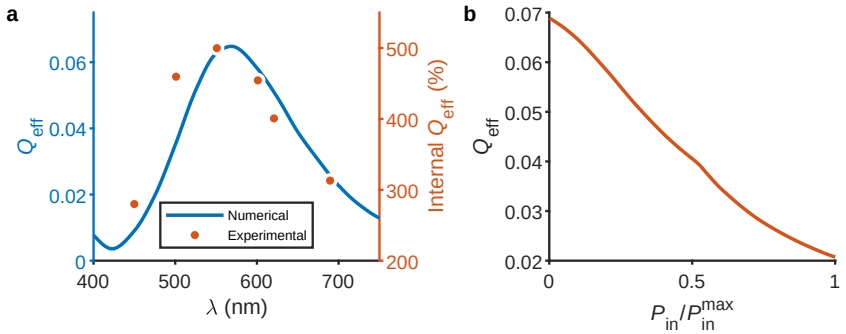

Figure 3. a) Numerically calculated quantum efficiency as a function of wavelength (left y-axis) at $P = 0.2$ μW and experimentally obtained internal quantum efficiency (right y-axis). b) Calculated quantum efficiency as a function of normalized incident illumination power at $V_d = 0.2$ V, $V_g = 10$ V, and $\lambda = 561$ nm.

We have numerically calculated the phase noise of the monolayer MoS_2-based phototransistor by following the method described in Ref. 23. Figures 4 (a) and (b) illustrate the phase noise as a function of wavelength and incident power, respectively. It is observed that the phase noise increases with wavelength and decreases with incident power. This is because phase noise depends on the output power. Since at higher wavelengths, the output current is reduced due to the lower absorption coefficient of monolayer MoS_2; phase noise is increased. Similarly, the output current increases with incident illumination, as shown in Fig. 2. Therefore, it reduces the phase noise. One crucial fact is that the wavelength of minimum phase noise in the visible spectrum (~ 430 nm) is different from the wavelength of maximum Q_{eff} (~ 561 nm).

Finally, we analyze the device's RF output power and bandwidth.[19] We modulate the generation rate of the MoS_2 monolayer by using the following expression: $G_{\text{in}} = G[1 + m\sin(2\pi f_{\text{mod}} t)]$, where m represents the modulation depth and f_{mod} is the modulation frequency. Using this expression, we find the output current

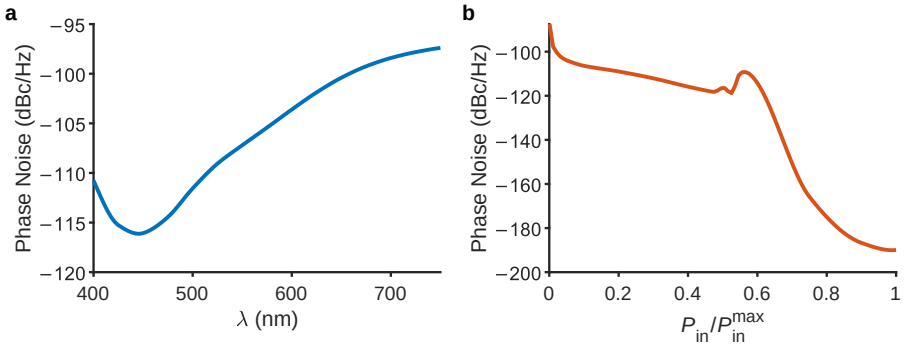

Figure 4. Calculated phase noise as a function of a) illumination wavelength at $P = 0.2$ μW and b) normalized incident illumination power at $\lambda = 561$ nm. For both (a) and (b), $V_d = 0.2$ V, $V_g = 10$ V, and $\lambda = 561$ nm are set.

at various modulation frequencies. The output current is then used to calculate the RF output power using $P_{\mathrm{RF}} = I_{\mathrm{out}}^2 \times R_{\mathrm{Load}}$. The frequency change for which the power is reduced by 3 dB gives us the overall bandwidth of the device. We have calculated the RF output power and bandwidth for two types of dimensions: 1 μm $\times$ 1 μm and 40 μm $\times$ 40 μm. The numerical results are shown in Fig. 5. The numerically calculated bandwidth of the device in Fig. 5 (a) is approximately 1.16 GHz, which is slightly lower than the one reported in Ref. 14. Meanwhile, the 40 μm $\times$ 40 μm has a bandwidth of approximately 41.43 MHz.

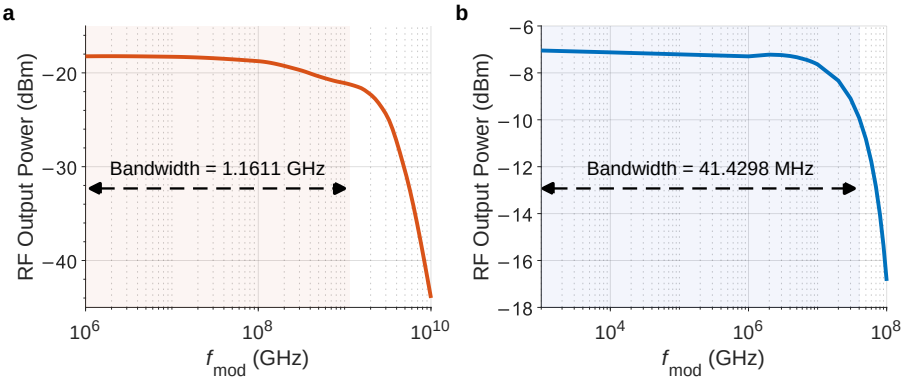

Figure 5. RF output power and total bandwidth of the device as a function of modulation frequency at $\lambda = 561$ nm, $V_d = 0.2$ V, and $V_g = 10$ V.

5. CONCLUSION

We have demonstrated a numerical solution for characterizing 2D material-based photodetectors. Different performance metrics have been analyzed for monolayer MoS_2 as the semiconducting channel using a 1D drift-diffusion model and a layered media approach. Alignment with experimental results found in the literature ensures the accuracy of the modeling technique. This solver enables us to compute the characteristics of this specific class of devices before going into fabrication, enhancing the process's efficiency.

REFERENCES

[1] Mak, K. F., Lee, C., Hone, J., Shan, J., and Heinz, T. F., "Atomically thin MoS_2: A new direct-gap semiconductor," *Phys. Rev. Lett.* **105**, 136805 (Sep 2010).

[2] Manzeli, S., Ovchinnikov, D., Pasquier, D., Yazyev, O. V., and Kis, A., "2D transition metal dichalcogenides," *Nature Reviews Materials* **2**, 17033 (2017).

[3] Lin, J., Li, H., Zhang, H., and Chen, W., "Plasmonic enhancement of photocurrent in MoS_2 field-effect-transistor," *Applied Physics Letters* **102**, 203109 (05 2013).

[4] Gupta, A., Sakthivel, T., and Seal, S., "Recent development in 2D materials beyond graphene," *Progress in Materials Science* **73**, 44–126 (2015).

[5] Lopez-Sanchez, O., Lembke, D., Kayci, M., Radenovic, A., and Kis, A., "Ultrasensitive photodetectors based on monolayer MoS_2," *Nature Nanotechnology* **8**, 497–501 (2013).

[6] Islam, R., Anjum, I. M., Menyuk, C. R., and Simsek, E., "Study of an MoS_2 phototransistor using a compact numerical method enabling detailed analysis of 2D material phototransistors," *submitted to Scientific Reports* (May 2024).

[7] Pak, J., Lee, I., Cho, K., Kim, J.-K., Jeong, H., Hwang, W.-T., Ahn, G. H., Kang, K., Yu, W. J., Javey, A., Chung, S., and Lee, T., "Intrinsic optoelectronic characteristics of MoS_2 phototransistors via a fully transparent van der Waals heterostructure," *ACS Nano* **13**(8), 9638–9646 (2019).

[8] Mukherjee, B., Tseng, F., Gunlycke, D., Amara, K. K., Eda, G., and Simsek, E., "Complex electrical permittivity of the monolayer molybdenum disulfide (MoS_2) in near UV and visible," *Opt. Mater. Express* **5**, 447–455 (Feb 2015).

[9] Korn, T., Heydrich, S., Hirmer, M., Schmutzler, J., and Schüller, C., "Low-temperature photocarrier dynamics in monolayer MoS_2," *Applied Physics Letters* **99**, 102109 (09 2011).

[10] Cheiwchanchamnangij, T. and Lambrecht, W. R. L., "Quasiparticle band structure calculation of monolayer, bilayer, and bulk MoS_2," *Phys. Rev. B* **85**, 205302 (May 2012).

[11] Simsek, E. and Mukherjee, B., "Visibility of atomically-thin layered materials buried in silicon dioxide," *Nanotechnology* **26**, 455701 (oct 2015).

[12] Salehzadeh, O., Tran, N. H., Liu, X., Shih, I., and Mi, Z., "Exciton kinetics, quantum efficiency, and efficiency droop of monolayer MoS_2 light-emitting devices," *Nano Letters* **14**(7), 4125–4130 (2014).

[13] He, G. et al., "Conduction mechanisms in CVD-grown monolayer MoS_2 transistors: From variable-range hopping to velocity saturation," *Nano Letters* **15**(8), 5052–5058 (2015). PMID: 26121164.

[14] Li, Z., Hu, S., Zhang, Q., Tian, R., Gu, L., Zhu, Y., Yuan, Q., Yi, R., Li, C., Liu, Y., Hao, Y., Gan, X., and Zhao, J., "Telecom-band waveguide-integrated MoS_2 photodetector assisted by hot electrons," *ACS Photonics* **9**, 282–289 (01 2022).

[15] Ueda, A., Zhang, Y., Sano, N., Imamura, H., and Iwasa, Y., "Ambipolar device simulation based on the drift-diffusion model in ion-gated transition metal dichalcogenide transistors," *Npj Comput. Mater.* **6** (2020).

[16] Chen, W., Yin, W.-Y., Zhao, W.-S., Hao, R., Li, E., Kang, K., and Guo, J., "Scaling analysis of high gain monolayer MoS_2 photodetector for its performance optimization," *IEEE Transactions on Electron Devices* **63**(4), 1608–1614 (2016).

[17] Mukherjee, B., Kaushik, N., Tripathi, R. P. N., Joseph, A. M., Mohapatra, P. K., Dhar, S., Singh, B. P., Kumar, G. V. P., Simsek, E., and Lodha, S., "Exciton emission intensity modulation of monolayer MoS_2 via Au plasmon coupling," *Scientific Reports* **7**(1), 41175 (2017).

[18] Wilson, S. P. and Walker, A. B., "One- and two-dimensional models of the transient response of metal - semiconductor - metal photodetectors including diffraction," *Semiconductor Science and Technology* **12**, 1265–1272 (1999).

[19] Simsek, E., Anjum, I. M., Carruthers, T. F., Menyuk, C. R., Campbell, J. C., Tulchinsky, D. A., and Williams, K. J., "Fast evaluation of RF power spectrum of photodetectors with windowing functions," *IEEE Transactions on Electron Devices* **70**(7), 3643–3648 (2023).

[20] English, C. D., Shine, G., Dorgan, V. E., Saraswat, K. C., and Pop, E., "Improved contacts to MoS_2 transistors by ultra-high vacuum metal deposition," *Nano Letters* **16**, 3824–3830 (06 2016).

[21] Gong, C., Zhang, H., Wang, W., Colombo, L., Wallace, R. M., and Cho, K., "Band alignment of two-dimensional transition metal dichalcogenides: Application in tunnel field effect transistors," *Applied Physics Letters* **103**, 053513 (08 2013).

[22] Blakemore, J., "Approximations for fermi-dirac integrals, especially the function $f_{1/2}(\eta)$ used to describe electron density in a semiconductor," *Solid-State Electronics* **25**(11), 1067–1076 (1982).

[23] Mahabadi, S. E. J., Wang, S., Carruthers, T. F., Menyuk, C. R., Quinlan, F. J., Hutchinson, M. N., McKinney, J. D., and Williams, K. J., "Calculation of the impulse response and phase noise of a high-current photodetector using the drift-diffusion equations," *Opt. Express* **27**, 3717–3730 (Feb 2019).